On the Origin of Amphiphilic Interfaces

Mohammed Bin Jassar* and Simone Pezzotti*

Laboratoire CPCV, Département de Chimie, École Normale Supérieure, PSL University, Sorbonne University, CNRS, 75005 Paris, France

E-mail: mohammed.bin-jassar@ens.psl.eu; simone.pezzotti@ens.psl.eu

Abstract

Solid/water interfaces are classified based on macroscopic textbook definitions of hydrophobicity and hydrophilicity. However, at the molecular level, increasing evidence reveals that whether an aqueous interface is hydrophobic or hydrophilic is not a binary question. Outlier interfaces that exhibit both hydrophilic and hydrophobic characteristics keep being dug out at a growing rate. These interfaces are strikingly diverse, ranging from metals to oxides, from conductors to insulators. We show that, despite their diversity, they can be united within a single family of systems with well-identified physical-chemical properties. In analogy to amphiphilic solutes, we name this family "amphiphilic interfaces". Amphiphilic interfaces possess remarkable wetting and solvation properties, with exciting potential applications in heterogeneous catalysis, geochemistry, nanofluidics, and electrochemistry. To unravel the origin of their atypical behavior, we trace the domain of amphiphilic interfaces as a function of relevant surface properties through extensive molecular dynamics simulations. Our findings elucidate why amphiphilic behavior arises across such a broad spectrum of surfaces, providing a unified framework to rationalize — and in the future control — the many intriguing properties that we keep discovering for these unique systems.

Introduction

Many physical and chemical processes on our planet and in industry occur at aqueous interfaces, where liquid water meets a solid surface.[1–3] The termination and reorganization of the water H-bond network in contact with a surface profoundly influence properties such as wetting,[4–8] surface speciation/hydroxylation,[2,9] adsorption and transport of ions and molecules,[10–14] energy transfer,[15–18] and the outcome of many chemical reactions.[1–3,19,20] Decades of intensive research traced the landscape of aqueous interfaces. With increasing solute-surface interaction strength, a transition from hydrophobic to hydrophilic interfaces is observed, which is subtly modulated by context-dependent parameters such as surface topology and morphology.[4,7,21–29] Such transition is marked by changes in contact angle at the macroscopic scale and local water density fluctuations (as measured by cavitation free energy) at the molecular scale, the two being quantitatively related.[5] Water density fluctuations are enhanced at hydrophobic interfaces (high contact angle), while suppressed at hydrophilic interfaces (low contact angle). The hydrophobic–hydrophilic transition is accompanied by a drastic change in the above-mentioned interfacial properties, which influence an enormous variety of fields.[2,3,14,20,21,26,28,30–33]

In the last decade, a growing number of studies reported interfaces that do not fit into the established picture: they exhibit an atypical behavior with mixed properties of both hydrophilic and hydrophobic interfaces.[8,11,13,34–39] Fascinating wetting and solvation properties are being dug out for many of these interfaces, with promising applications in heterogeneous catalysis, geochemistry, prebiotic chemistry, and electrochemistry, to cite a few.[8,11–13,32,34,37,39–41] Intriguingly, these interfaces have apparently little in common with each other - they range from geochemical to electrochemical, from metals to oxides, from conductors to insulators.

The first report was on talc surfaces.[34] There, individual water molecules adsorb strongly (hydrophilic behavior) at low relative humidity due to adhesive surface–water interactions; however, at saturation, a droplet of water beads on the surface, as typical for hydrophobic

interfaces. Rotenberg et al.[34] rationalized this duality in terms of a competition between adhesion and cohesion (water–water interactions). Surprisingly, they noted that a water droplet forms on top of a strongly adsorbed water monolayer (adlayer), even on the most adhesive surfaces. For rutile, Molecular Dynamic (MD) simulations, contact angle measurements, and Sum Frequency Generation (SFG) spectroscopy by Qu et al.[35] proved the surface is strongly wet by a water bilayer. However, the addition of more water results in the formation of a droplet with a finite contact angle on top of it, which led the authors to question whether the interface is hydrophilic or hydrophobic. Experimental measurements of water adsorption enthalpy on alpha-(0001)-quartz surfaces reported strongly exothermic adsorption of a 1^{st} water monolayer, as typical of very hydrophilic surfaces.[36] This is due to strong H-bonding between quartz SiOH terminations and water, as confirmed by several MD and SFG studies.[2] However, the addition of a 2^{nd} water layer was surprisingly found much less exothermic and to leave the 1^{st} monolayer structure virtually unperturbed.

At Pt/water interfaces, Limmer, Willard et al.[8,37] initiated a quest on how hydrophobic properties – such as enhanced density fluctuations – arise despite strong metal–water interactions, due to the ordering of the water adlayer on top of the metal. We could later show[11,42] for Au/water interfaces that strong metal–water interactions template a very ordered water adlayer, where intra-layer water–water H-bonds and interactions with the surface are both maximized. This leaves few spots available for H-bonding between the adlayer and the adjacent water layer. Hence, next to the hydrophilic metal-adlayer interface, where density fluctuations are suppressed, a water–water interface with a low H-bond density is formed, where water density fluctuations are enhanced, as typical of hydrophobic interfaces.

The dual hydrophobic/hydrophilic nature was recognized to dictate many properties of metal/aqueous interfaces, including adsorption and transport of reactive species across the interface,[8,11,42] the outcome of several chemical reactions,[39,40,43] acid-base chemistry,[32] as well as the properties of the Electric Double Layer.[12,37,44] Most recently, Gäding et al.[13] discussed how the degree of ordering within the adlayer formed on top of many metal and

other surfaces also dictates friction and osmotic transport at the interface. Independently, Li et al.[41] proposed that the low H-bond density at the water–water interface close to the metal limits proton transport across the interface and dominates the kinetic pH effect in hydrogen electrocatalysis.[41,45]

Here, we propose a picture that allows us to unite all these diverse interfaces and observations within a single family of systems. We name this family "amphiphilic interfaces", whose common trait is – in analogy to amphiphilic solutes – to display both a hydrophilic and a hydrophobic side. This picture is derived from extensive MD simulations that allow tracing the domain of amphiphilic interfaces as a function of relevant surface parameters, namely surface–water interaction strength, metallicity, applied voltage, and surface topology.

Results and Discussions

Which surface properties unlock the amphiphilic behavior? We employed constant potential MD[46] to simulate a series of interfaces derived from an Au(100)/water system by changing the properties of the "Au" electrode. An Au(100) electrode is chosen as the starting point because, despite being reported for a great diversity of systems, amphiphilic behaviors have been extensively characterized at Au(100).[11,13,38,40,42] The surface properties suspected to be relevant are: (i) the strength of adhesive surface–water interactions, since amphiphilic behavior was observed for strongly adhesive surfaces; (ii) surface metallicity, as amphiphilicity was intriguingly observed for both insulators and conductors; (iii) applied voltage, as many amphiphilic interfaces are electrified. Adhesive surface–water interactions were tuned by the ϵ parameter in the Lennard-Jones potential between Au and water (O-atom). Metallicity was tuned by changing the width (σ) of the Gaussian charge distribution used to represent the atomic charges in Au:[47] a larger Gaussian width corresponds to a more metallic (more conductive) surface. The applied voltage was varied within the water electrochemical window, from the point of zero charge (PZC = 0 V) to −0.5 V on the negative

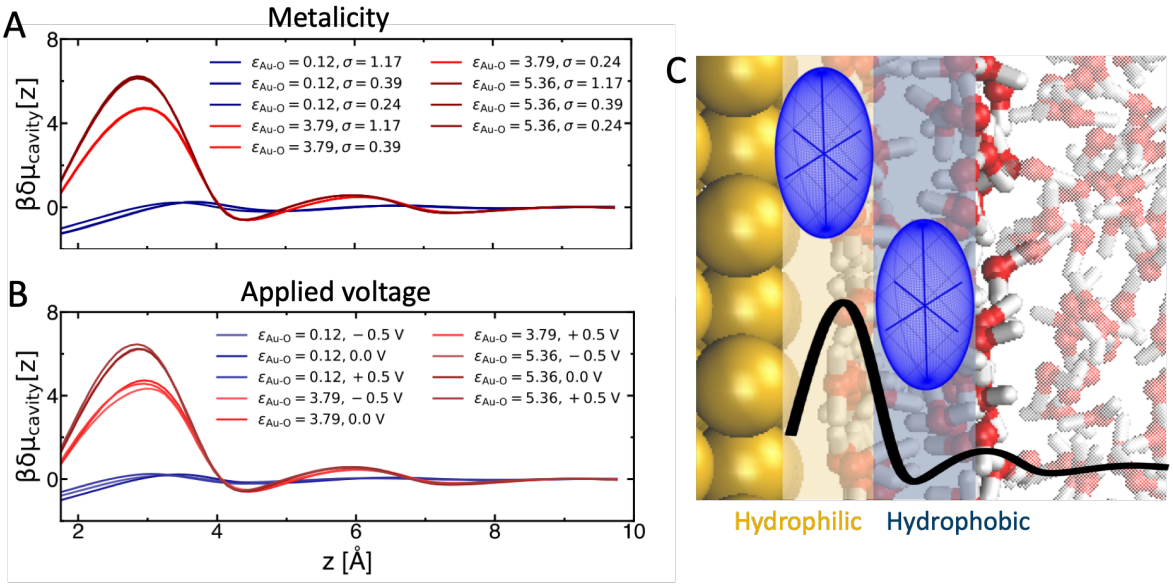

Figure 1: Mapping amphiphilic interfaces as a function of surface properties. (A) and (B) compare the effect of surface–water interaction strength (ϵ_{Au-O} in kJ/mol) *vs* surface metallicity (σ in Å) and applied voltage (ΔV), respectively. Amphiphilic behavior is quantified by cavitation free energy ($\delta\mu_{cavity}$) profiles along the z distance from the surface. $\delta\mu_{cavity}(z)$ monotonically decreases when approaching a hydrophobic surface, as in the profiles with $\epsilon_{Au-O} = 0.12$ kJ/mol (blue curves). Amphiphilic behavior is observed for the two high ϵ_{Au-O} values, independently of metallicity and voltage. (C) Illustration of the amphiphilic behavior at Au/water (red oxygen and white hydrogen). The black curve shows the typical oscillating $\delta\mu_{cavity}(z)$ profile (for the illustrated ellipsoidal cavity, see methods), with exceptionally high $\delta\mu_{cavity}(z)$ at the hydrophilic surface-adlayer interface, and a minimum at the adjacent water-water interface.

side and to +0.5 V on the positive side.

The influence of these surface properties is evaluated by analysis of water density fluctuations (as quantified by cavitation free energies), which provide a well-established measure of local hydrophobicity:[4,5,8,11,21,48,49] the free energy cost to spontaneously form a small cavity in the liquid is reduced compared to bulk water at hydrophobic interfaces ($\delta\mu_{cavity} < 0$) due to enhanced fluctuations of the water density, while $\delta\mu_{cavity} \geq 0$ at hydrophilic interfaces. $\delta\mu_{cavity}(z)$ profiles along the z distance from the surface (where δ identifies a difference between the z-position at the interface and the bulk) were computed from the MD simulations (see methods). Corresponding contact angle values were deduced with the approach of ref. 5 and are shown in the SI.

Fig.1-A and -B compare the effect of adhesive interactions *vs* metallicity and applied voltage, respectively. Strikingly, adhesion emerges as the dominant parameter, while comparably smaller modulations of $\delta\mu_{cavity}(z)$ arise from the surface being insulator/conductor or neutral/charged. At low interaction strength (ϵ_{Au-O}= 0.12 kJ/mol) , we systematically recover the typical $\delta\mu_{cavity}(z)$ profile of a hydrophobic interface: $\delta\mu_{cavity}(z)$ monotonically decreases when approaching the surface.[21,48] Instead, for interaction strength equal (ϵ_{Au-O}= 3.79 KJ/mol) or higher (ϵ_{Au-O}= 5.36 KJ/mol) than for the original Au(100) surface, the amphiphilic behavior arises, independently of metallicity and applied voltage. As illustrated in Fig.1-C, this is characterized by exceptionally high $\delta\mu_{cavity}(z)$ at the hydrophilic interface formed between the surface and the water adlayer (z< 3.5 Å), where there is a high density of water-surface interactions and intra-adlayer water–water H-bonds.[42] Instead, $\delta\mu_{cavity}(z)$ becomes negative (i.e., hydrophobic-like) at the adjacent water–water interface, where the density of inter-layer H-bonds between the adlayer and the adjacent water layer is low. These results rationalize why amphiphilicity was observed for both insulators and conductors, electrified and neutral surfaces: it can manifest with sufficiently strong surface–water interactions, independently of the nature of the surface.

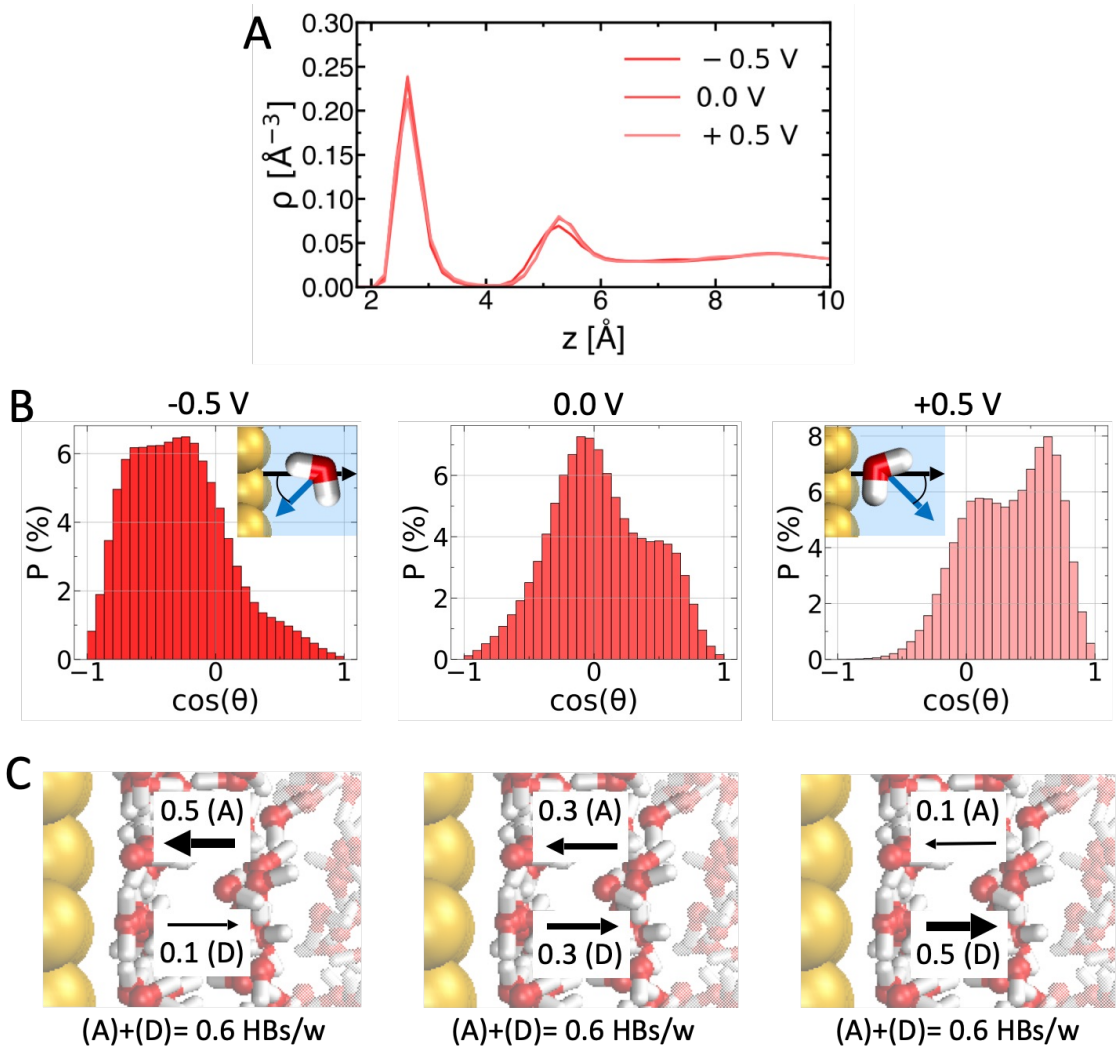

Figure 2: Why are ΔV variations within the water electrochemical window insufficient to induce/prevent amphiphilic behavior. (A) ΔV induced changes in water oxygen density profiles (for $\epsilon_{Au-O} = 3.79$ kJ/mol and $\sigma = 1.17$ Å). (B) Water dipole orientation (Cos θ, see scheme) distributions for different ΔV. (D) Accompanying changes in the number of H-bonds per water molecule (HBs/w) formed between the adlayer and the adjacent layer: adlayer water mostly receives HBs (0.5 *vs* 0.1 HBs/w) from water in the next layer at $\Delta V = -0.5$ V, while it mostly donates HBs at $\Delta V = +0.5$ V. However, the total density of HBs/w – that dictates $\delta\mu_{cavity}(z)$ – remains constant (0.6 HBs/w). Error bars on HBs/w values are $< \pm$ 0.05 HBs/w.

This may appear surprising at first glance, since both metallicity and applied voltage influence the way water molecules interact with the surface and with themselves.[11,47,50] To understand this, we characterize the effect of applied voltage on the interfacial water H-bond network in Fig.2. Tuning the voltage across the PZC does not substantially influence the

water oxygen density profile (Fig.2-A), in particular the height and position of the first density peak corresponding to the water adlayer. However, it strongly alters the orientation of water molecules within the adlayer (Fig.2-B): water molecules are mostly oriented with their dipole parallel to the surface at PZC= 0 V (probability maximum for $\cos\,\theta \simeq 0$), but reorient pointing their dipole toward the negative surface ($\cos\,\theta < 0$ for –0.5 V) and away from the positive surface ($\cos\,\theta > 0$ for +0.5 V). As shown in Fig.2-C, the reorientation alters inter-layer H-bonding at the water–water interface: adlayer water mostly accepts H-bonds from water in the subsequent layer at negative voltage, while it mostly donates at positive voltage. However, the total density of H-bonds remains constant. Since what matters for density fluctuations is the density of H-bonds that has to be perturbed to create a cavity, $\delta\mu_{cavity}(z)$ is not very sensitive to applied voltage variations. A similar molecular rationalization applies for the effect of metallicity, too (Fig.S1 in the SI).

Locating the crossover from hydrophobic to hydrophilic to amphiphilic. Leveraging on the gained knowledge, we can anticipate that, if such a crossover exists, it must appear with increasing surface–water interaction. We hence examine in Fig.3 how the structure of the interface and $\delta\mu_{cavity}(z)$ change by continuously varying ϵ_{Au-O} (as shown in Fig.3-A with the corresponding Lennard-Jones potentials) from the value of 0.12 kJ/mol, for which we observed hydrophobic behavior, to the value of 5.36 kJ/mol (amphiphilic behavior). The larger ϵ_{Au-O}, the more the water (O-atom) density profile (Fig.3-B) becomes structured at the solid-liquid interface, with the progressive appearance of a 1^{st} density peak at around 2.8 Å , indicative of the formation of a water adlayer, followed by a depleted inter-layer region and by a 2^{nd} density peak. Concomitantly (inset), the number of intra-layer H-Bonds formed between adlayer water molecules increases (red curve), while that of inter-layer H-bonds formed by the adlayer with the water molecules in the 2^{nd} layer decreases (blue), until both reach a plateau at $\epsilon_{Au-O} \simeq 3$ kJ/mol. At the plateau, the connectivity within the adlayer is maximized, which corresponds to the fewest amount of spots remaining available for

H-bonding with the 2^{nd} layer. From the density profiles, we can quantify the water chemical potential at the interface: $\delta\mu_{water}(z) = -lnP_w(z)$, with $P_w(z)$ being the probability to find a water molecule at a given z-distance from the surface (normalized by tha in the bulk). With increasing ϵ_{Au-O}, water adsorption in the adlayer (1^{st} minimum in the $\delta\mu_{water}(z)$ profiles) becomes more favorable, boosted by the increased water–water connectivity, while the free energy barrier to remove a water molecule from the adlayer ($\delta\mu_{adlayer}$, i.e., the difference between the 1^{st} $\delta\mu_{water}$ minimum and the subsequent maximum) increases. These changes appear smooth and continuous.

Strikingly, they are accompanied by a continuous crossover from $\delta\mu_{cavity}(z)$ profiles typical of hydrophobic interfaces (blue in Fig.3-D) to $\delta\mu_{cavity}(z)$ profiles typical of an amphiphilic interface (red/brown). This is marked by the progressive appearance of a $\delta\mu_{cavity}$ maximum at z<3.5 Å (where the cavity is formed inner-sphere, i.e., in direct contact with the surface and within the adlayer) and a minimum at ∼4.5 Å (where the cavity is formed outer-sphere, i.e., at the adjacent water–water interface where it is separated from the surface by the adlayer). These changes are quantified in Fig.3-E by plotting the $\delta\mu_{cavity}$ values at ∼1.8 Å (red, inner-sphere) and at ∼4.5 Å (blue, outer-sphere) as a function of ϵ_{Au-O}. At low ϵ_{Au-O}, inner-sphere is more favorable than outer-sphere cavity formation, and both are favored with respect to bulk ($\delta\mu_{cavity} < 0$). This indicates hydrophobic behavior, as $\delta\mu_{cavity}$ monotonically decreases when approaching a hydrophobic surface.[21,48] With increasing ϵ_{Au-O}, the $\delta\mu_{cavity}$ value for inner-sphere increases, approaches zero, and becomes positive, while crossing with the decreasing value for outer-sphere (at around ϵ_{Au-O} = 2 kJ/mol in our model). In this range, $\delta\mu_{cavity}$ for inner-sphere, outer-sphere and bulk are most similar to each other, which is typical of hydrophilic interfaces.[21,39,48] This is the canonical hydrophobic–hydrophilic transition. However, when further increasing surface–water interactions, inner- and outer-sphere $\delta\mu_{cavity}$ diverge, and the interface progressively partition into a hydrophilic side (the surface-adlayer interface) and a hydrophobic side (the subsequent water–water interface), giving rise to the amphiphilic behavior.

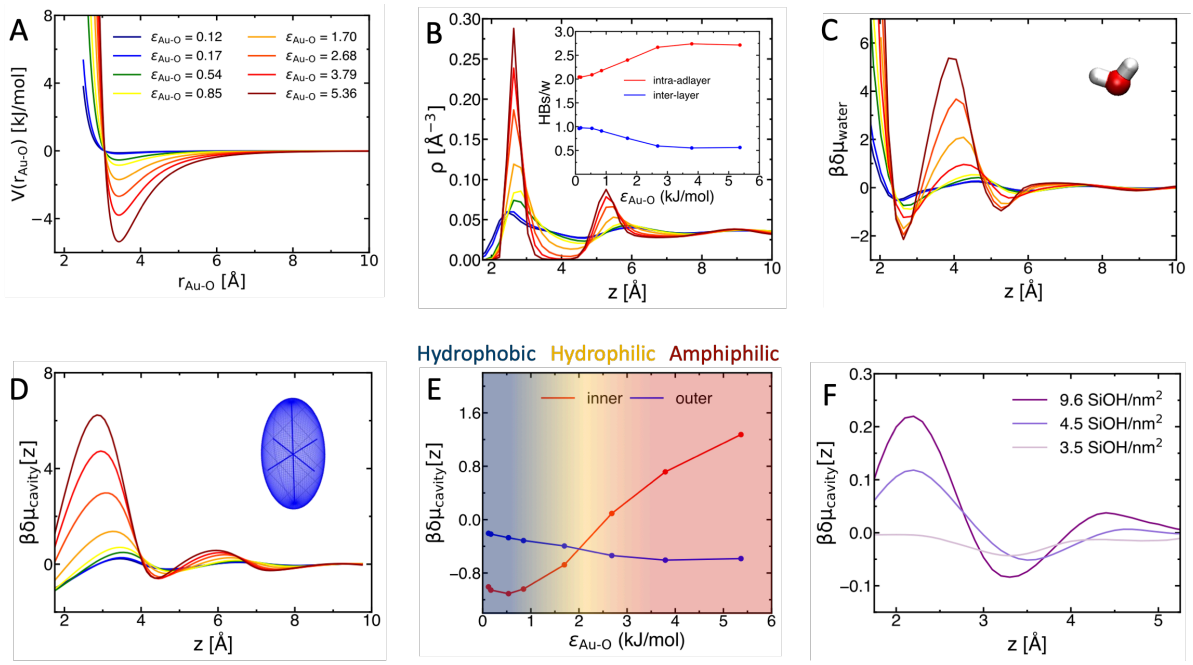

Figure 3: The hydrophobic-hydrophilic-amphiphilic crossover with increasing surface–water interactions, ϵ_{Au-O}. (A) Lennard-Jones potential $V(r_{Au-O})$ for each ϵ_{Au-O}. (B) Water Oxygen density profiles, showing the progressive appearence of an ordered water adlayer (1^{st} density peak). (Inset) Accompanying changes in the number of water-water H-bonds (HBs/w) formed within the adlayer (red) and between the adlayer and the adjacent water layer (blue). (C) Water chemical potential $\delta\mu_{water}$ across the interface, as computed from the density profiles. (D) $\delta\mu_{cavity}(z)$ profiles (see Fig. S2 in SI for the corresponding changes in contact angle, which varies from 90^o to full wetting with increasing ϵ_{Au-O}). (E) $\delta\mu_{cavity}(z)$ changes are quantified by plotting the values at z= 1.8 Å (inner) and 4.5 Å (outer) as a function of ϵ_{Au-O}. The color gradient highlights the progressive crossover: $\delta\mu_{cavity}(z)$ inner $<$ outer at a hydrophobic interface (blue), inner $\simeq$ outer at a hydrophilic interface (orange), and inner $>$ outer at an amphiphilic interface (brown). (E) The hydrophilic-amphiphilic crossover is also observed for silica–water interfaces, where the adhesive force is increased by increasing surface hydroxylation rate (SiOH/nm^2) instead of ϵ_{Au-O}, showing the generality of our findings.

A progressive hydrophilic–amphiphilic crossover hence takes place when maximizing surface adhesion by increasing the attractive interaction between surface site and water molecule. This is typically the way surface adhesion varies across metal surfaces, e.g., from Au to Cu to Pt.[51,52] However, this does not apply to oxides, for which amphiphilic behaviors have been reported, too.[34–36,39] There, the adhesive interactions are primarily modulated by the amount of surface (-OH) terminations that interact strongly with water. A typical exam-

ple are silica/water interfaces, where surface adhesion increases monotonically with the degree of hydroxilation, i.e., the density of surface SiOH termination that form strong H-bonds with water (which is tuned by changing the way the surface is heat-treated).[28,53] To explore the generality of our findings, we also performed our analysis on three well-characterized silica surfaces with increasing hydroxylation rate of 3.5 SiOH/nm^2, 4.5 SiOH/nm^2 and 9.6 SiOH/nm^2 (from previously performed DFT-MD simulations[39]). These model systems were shown to reproduce well the properties of heat treated amorphous silica, amorphous silica and α-(0001)-quartz surfaces in contact with liquid water, respectively.[28,39,53] The corresponding $\delta\mu_{cavity}(z)$ profiles (Fig.3-F) show again a smooth, continuous crossover from a canonical hydrophilic behavior (3.5 SiOH/nm^2), with similar $\delta\mu_{cavity}(z)$ values in inner-, outer-sphere and bulk, to the amphiphilic quartz/water interface (9.6 SiOH/nm^2), where the hydrophilic and hydrophobic sides (with suppressed and enhanced density fluctuations, respectively) emerge.[39] We show in Table S1 of the SI that the hydrophilic–amphiphilic transition is, also in this case, accompanied by an increasing connectivity within the adlayer and decreasing H-bonding between the adlayer and the second water layer. The hydrophilic–amphiphilic crossover is accessible independently of the way surface adhesion is increased.

Understanding the crossover. Fig.4 shows that such crossover is quantitatively dictated by the surface induced structural changes in the surface-adlayer and water–water sides of the interface. As discussed above, local hydrophobicity, i.e. the value of $\delta\mu_{cavity}(z)$, depends on the number and strength of water–water and surface–water interactions that have to be perturbed to form a small cavity. For a cavity inscribed in the water–water interface, this cost in dictated by the inter-layer water–water H-bonds, which all have similar strength. The number of such H-bonds (HBs/w) is – to a good approximation – linearly proportional to the local $\delta\mu_{cavity}$ (Fig.4-A). Starting from the least adhesive, most hydrophobic surface, increasing ϵ_{Au-O} induces more ordering within the adlayer, with fewer spots remaining available for inter-layer H-bonding with the 2^{nd} water layer, causing both HBs/w and $\delta\mu_{cavity}$

to decrease. Once the adlayer structure is fully ordered and does not change anymore with ϵ_{Au-O} (at $>$ 3 kJ/mol in our model), the number of inter-layer HBs/w reaches a plateau, and so does the local $\delta\mu_{cavity}$.

At the surface-adlayer interface (Fig.4-B), cavity formation requires displacing water molecules from the ordered adlayer structure, which involves perturbing both surface–water and intra-adlayer water–water HBs. Here, $\delta\mu_{cavity}$ is dictated by surface desolvation, i.e. by the free energy cost to remove water molecules from the adlayer ($\delta\mu_{adlayer}$).[38,40,42,54] At low ϵ_{Au-O}, in the hydrophobic domain, water-surface interactions are weaker than water–water H-bonds and the adlayer structure is only little sensitive to the ϵ_{Au-O} increase. Thus, both $\delta\mu_{adlayer}$ and local $\delta\mu_{cavity}$ are almost insensitive to changes in surface adhesion, until surface–water overcomes water–water interactions (at $\epsilon_{Au-O} \simeq 1.5$ kJ/mol in our model). After that, both the strength of water-surface interactions and the number of intra-adlayer HBs/w monotonically increase with ϵ_{Au-O}, causing $\delta\mu_{adlayer}$ and $\delta\mu_{cavity}$ to increase. Upon entering the amphiphilic domain, the number of intra-adlayer HBs/w saturates, but $\delta\mu_{adlayer}$ and $\delta\mu_{cavity}$ keep increasing due to the continuous increase in surface adhesion. Therefore, the mechanism of the crossover is the following. For hydrophobic interfaces, water–water interactions dominate and increasing surface adhesion has little effect on wetting properties until surface–water overcomes water–water interactions. In the hydrophilic domain, the more adhesive the surface, the more ordered the water adlayer, the lower the inter-layer H-bond density in the adjacent water–water region. These structural changes progressively cause density fluctuations in the two regions to diverge, with formation of a locally superhydrophilic surface-adlayer interface followed by a locally hydrophobic water–water interface.

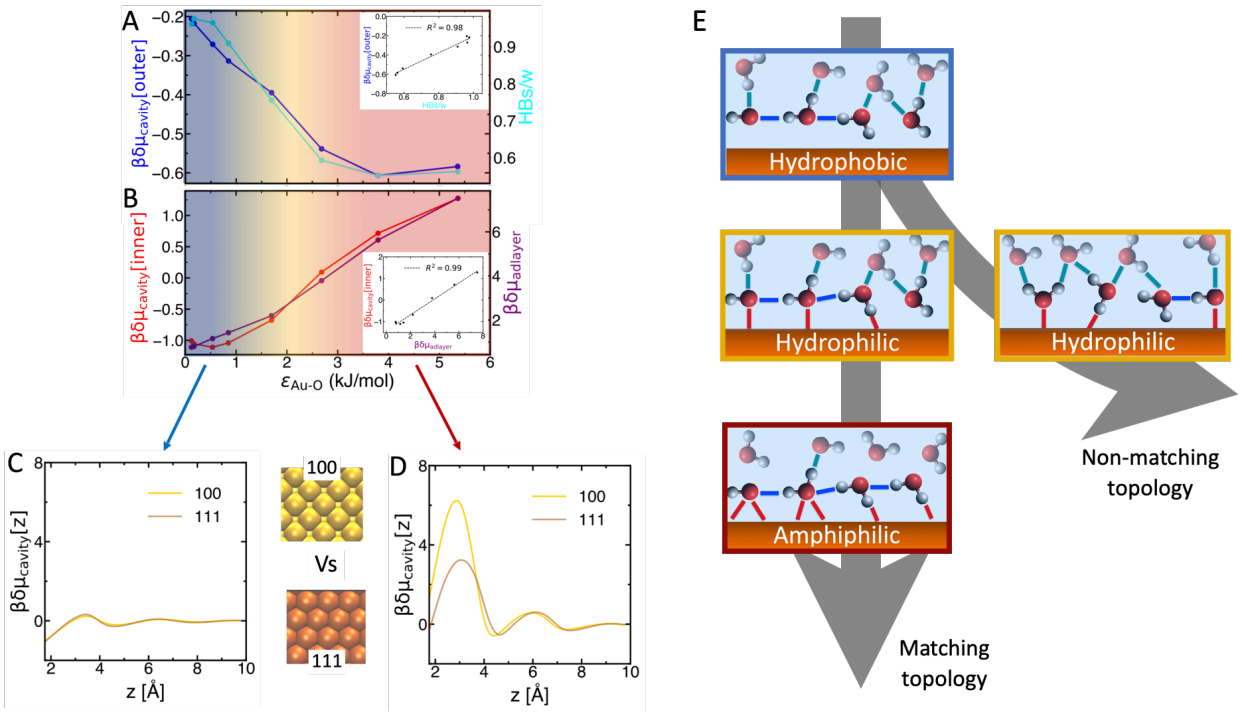

Figure 4: Molecular understanding of the crossover. (A) $\delta\mu_{cavity}(z)$ changes vs ϵ_{Au-O} at the hydrophobic water–water side of the interface (from Fig.3-E, outer) are dictated by changes in the number of inter-layer H-bonds (HBs/w, Fig.3-B). The inset highlights the linear correlation between the two. (B) $\delta\mu_{cavity}(z)$ changes at the hydrophilic side (inner) are dictated by the free energy cost to displace a water molecule from the adlayer ($\delta\mu_{adlayer}$), which depends on both water-surface and water-water interactions. The inset correlates $\delta\mu_{cavity}$(inner) with $\delta\mu_{adlayer}$. (C) and (D) Effect of surface topology at different sides of the crossover, evaluated by comparing $\delta\mu_{cavity}(z)$ profiles at Au(100) and Au(111) derived surfaces with same ϵ_{Au-O}, $\sigma = 1.17$ Å, and $\Delta V = 0$ V, for $\epsilon_{Au-O} = 0.12$ kJ/mol (C, hydrophobic), and $\epsilon_{Au-O} = 5.36$ kJ/mol (D, amphiphilic). (E) Updated understanding of aqueous interfaces, combining our results with recent literature. The arrows follow the crossover with increasing surface adhesion. The sketches illustrate the accompanying changes in surface-water (red lines), intra-adlayer (blue) and inter-layer (cyan) H-bonds. For increasingly adhesive surfaces, the newly discovered amphiphilic behavior can be reached, beyond the canonical hydrophobic–hydrophilic crossover, if the surface topology matches that of the water adlayer.

The effect of surface topology. The prerequisite to enter the amphiphilic domain is hence the formation of an ordered adlayer where both surface–water and water–water interactions are maximized. This requires the pattern on the surface to be commensurate

to the water network.[8,13,25,29,31] If not, the formation of surface–water interactions locally perturbs the water network, causing either the breaking or the (out-of-plane) reorientation of intra-adlayer water–water H-bonds, as described in many previous studies.[29,31,55–58] This prevents the formation of horizontally ordered adlayer structures, leading to canonical hydrophilic interfaces that cannot exhibit amphiphilic behaviors, as typical for most biological and oxide surfaces.[25,55,58] Hence, amphiphilic behaviors must be strongly modulated by surface topology, i.e. by the pattern formed by the surface sites that interact strongly with water. To explore the topology effect, we constructed model interfaces with the same ϵ_{Au-O}, metallicity, and applied voltage as for the Au(100) derived surfaces, but starting from a Au(111) surface, instead. Fig.4-C and -D compare $\delta\mu_{cavity}$ profiles at Au(100) *vs* Au(111) model surfaces in the hydrophobic and amphiphilic domains, respectively. Almost identical profiles are observed at low ϵ_{Au-O}: surface topology is almost irrelevant for hydrophobic interfaces, in agreement with ref. 58. This is rationalized by considering that water–water overcomes surface–water interactions; therefore, the interfacial water network is dictated by water–water H-bonds instead of adapting to the surface.[31,55,58,59]

The topology effect is remarkable in the amphiphilic domain, instead. The value of $\delta\mu_{cavity}$ at the hydrophilic surface–adlayer interface (z$<$ 4 Å) changes by a factor of two between Au(100) and Au(111). This large topology effect is in line with previous studies comparing the wetting of different facets of the same metal.[8,13,38] As shown by water density and $\delta\mu_{water}$ profiles in Fig.S3 of the SI, we find that surface topology dictates the degree of ordering within the adlayer, and as a consequence $\delta\mu_{adlayer}$. This, in turn, dictates the extent to which amphiphilic behaviors manifest. The effect of surface topology varies depending on where an interface is placed along the hydrophobic–hydrophilic–amphiphilic crossover.

Conclusion

In summary, we propose a framework to rationalize the growing number of diverse interfaces that defy binary hydrophobic or hydrophilic definitions, classifying them within a single family: amphiphilic interfaces. Amphiphilic interfaces are characterized by the coexistence of a locally hydrophilic (surface-adlayer) and hydrophobic (adlayer-2^{nd} layer) side. We identified adhesive surface–water interactions and surface topology as the key factors driving the amphiphilic behavior. As surface-water interaction increases, we traced the continuous transitions from hydrophobic to hydrophilic and then to amphiphilic interfaces using cavitation free energy analysis. As summarized in fig.4-E, the transition is governed by the surface-induced structural changes in both surface-adlayer and water–water sides of the interface. We show that amphiphilic behaviors can arise for both conductors and insulators, oxides and metals, as long the surface is able to induce a horizontally ordered adlayer structure. This depends on surface topology, as a good geometric match between surface and adlayer patterns is required to maximize surface-adlayer and intra-adlayer H-bonds simultaneously.

In the last decade, many studies[8,11–13,32,34,37,39–41,43,45] individually identified specific properties of either the hydrophilic or hydrophobic side of a diversity of amphiphilic interfaces to be key in regulating a variety of chemical-physical processes. These include the low H-bond density at the hydrophobic side of metal/water interfaces for proton transport and hydrogen evolution reaction in electrochemistry,[41] the degree of ordering within the adlayer for friction and osmotic flow in nanofluidics,[13] the difference in solvation free energies between hydrophobic and hydrophilic sides for heterogeneous catalysis and prebiotic chemistry,[32,39,40] and many more. The present work provides a unified ground to rationalize all these properties and the way they can be controlled by adjusting the interface composition. This may open exciting perspectives in interface science.

Methods

All simulations were performed using the constant potential classical MD code MetalWalls,[46] on a 3.66×3.66×7.00 nm box containing 2,381 SPC/E[60] water molecules confined between two identical planar Au electrodes of five atomic layers. 2D periodic boundary conditions were applied on x and y. For Au, Lennard-Jones parameters from Heinz et al.[52] were used, in combination with Lorentz-Berthelot mixing rules. For each simulation, the system was first equilibrated for 500 ps in the NVT ensemble at $T = 298$ K with a 1 fs timestep, followed by 500 ps in the NPT ensemble, where the electrodes acted as pistons to maintain constant pressure, until the system's density had converged. Then, NVT production runs were propagated with a 2 fs timestep for at least 30 ns.

We adopted the approach of ref. 47 to tune surface metallicity by the width of the atom-centered Gaussian charge distributions (σ) on the topmost electrode atoms as a function of the position r:

$$\rho_i(r) = q_i(2\pi\sigma^2)^{-3/2} e^{-\frac{|r-r_i|^2}{2\sigma^2}} \tag{1}$$

where $\rho_i(r)$ and r_i are the charge distribution and the position of the electrode atom i, respectively, while q is the atomic charge. Cavitation free energy profiles were obtained by computing the probability $P_{v,s}(0,z)$ of observing zero water Oxygen centers within the probing volume v (with shape s) at each z-distance from the surface.[8,11]

$$P_{v,s}\ (0,z) = e^{-\beta\ \Delta\mu_{v,s}(z)} \tag{2}$$

$$\delta\mu_{cavity}(z) = \ \Delta\mu^{int}_{v,s}\ (z) - \ \Delta\mu^{bulk}_{v,s} \tag{3}$$

where $\Delta\mu$ is the free energy cost of cavity formation, and $\beta = 1/\mathrm{k_B}T$. We systematically employed an ellipsoidal probing volume of 2.00×2.00×1.75 Å, which is small enough to fit

within the hydrophilic (and hydrophobic) side of an amphiphilic interface. This is essential to avoid mixing cavitation free energy contributions from the two sides, as detailed in ref. 42. H-bond analysis adopted the Luzar-Chandler distance+angle criterion.[61]

Supporting Information

Additional methodological details regarding the simulations performed for systems containing Au (111) and the three types of silica are provided. Additional analytical details are also included, examining the effects of metallicity and surface topology on the systems studied.

Acknowledgements

This work is funded by the European Research Council (ERC, ELECTROPHOBIC, Grant Agreement No. 101077129) . This work was performed using HPC resources from GENCI, allocation No. A0170802309. We thank Dr. Wanlin Chen for The Interesting And Motivating Opinions shared.

References

(1) Benjamin, I. Chemical reactions and solvation at liquid interfaces: A microscopic perspective. *Chem. Rev.* **1996**, *96*, 1449–1476.

(2) Bañuelos, J. L.; Borguet, E.; Brown Jr, G. E.; Cygan, R. T.; DeYoreo, J. J.; Dove, P. M.; Gaigeot, M.-P.; Geiger, F. M.; Gibbs, J. M.; Grassian, V. H.; others Oxide–and silicate–water interfaces and their roles in technology and the environment. *Chem. Rev.* **2023**, *123*, 6413–6544.

(3) Gonella, G.; Backus, E. H.; Nagata, Y.; Bonthuis, D. J.; Loche, P.; Schlaich, A.;

Netz, R. R.; Kühnle, A.; McCrum, I. T.; Koper, M. T.; others Water at charged interfaces. *Nat. Rev. Chem.* **2021**, *5*, 466–485.

(4) Chandler, D. Interfaces and the driving force of hydrophobic assembly. *Nature* **2005**, *437*, 640–647.

(5) Godawat, R.; Jamadagni, S. N.; Garde, S. Characterizing hydrophobicity of interfaces by using cavity formation, solute binding, and water correlations. *Proc. Natl. Acad. Sci.* **2009**, *106*, 15119–15124.

(6) Acharya, H.; Vembanur, S.; Jamadagni, S. N.; Garde, S. Mapping hydrophobicity at the nanoscale: Applications to heterogeneous surfaces and proteins. *Faraday Discuss.* **2010**, *146*, 353–365.

(7) Cheng, Y.-K.; Rossky, P. J. Surface topography dependence of biomolecular hydrophobic hydration. *Nature* **1998**, *392*, 696–699.

(8) Limmer, D. T.; Willard, A. P.; Madden, P.; Chandler, D. Hydration of metal surfaces can be dynamically heterogeneous and hydrophobic. *Proc. Natl. Acad. Sci. U.S.A.* **2013**, *110*, 4200–4205.

(9) Li, X.; Brigiano, F. S.; Pezzotti, S.; Liu, X.; Chen, W.; Chen, H.; Li, Y.; Li, H.; Lin, X.; Zheng, W.; others Unconventional structural evolution of an oxide surface in water unveiled by in situ sum-frequency spectroscopy. *Nat. Chem.* **2024**, 1–6.

(10) Tocci, G.; Joly, L.; Michaelides, A. Friction of water on graphene and hexagonal boron nitride from ab initio methods: very different slippage despite very similar interface structures. *Nano letters* **2014**, *14*, 6872–6877.

(11) Serva, A.; Salanne, M.; Havenith, M.; Pezzotti, S. Size dependence of hydrophobic hydration at electrified gold/water interfaces. *Proc. Natl. Acad. Sci. U.S.A.* **2021**, *118*, e2023867118.

(12) Alfarano, S. R. et al. Stripping away ion hydration shells in electrical double-layer formation: Water networks matter. *Proc. Natl. Acad. Sci.* **2021**, *118*, e2108568118.

(13) Gäding, J.; Della Balda, V.; Lan, J.; Konrad, J.; Iannuzzi, M.; Meißner, R.; Tocci, G. The role of the water contact layer on hydration and transport at solid/liquid interfaces. *Proc. Natl. Acad. Sci. U.S.A.* **2024**, *121*, e2407877121.

(14) Rogers, B. A.; Okur, H. I.; Yan, C.; Yang, T.; Heyda, J.; Cremer, P. S. Weakly hydrated anions bind to polymers but not monomers in aqueous solutions. *Nat. Chem.* **2022**, *14*, 40–45.

(15) Zhang, Z.; Piatkowski, L.; Bakker, H. J.; Bonn, M. Ultrafast vibrational energy transfer at the water/air interface revealed by two-dimensional surface vibrational spectroscopy. *Nat. Chem.* **2011**, *3*, 888–893.

(16) McGuire, J. A.; Shen, Y. R. Ultrafast vibrational dynamics at water interfaces. *Science* **2006**, *313*, 1945–1948.

(17) Yu, X.; Principi, A.; Tielrooij, K.-J.; Bonn, M.; Kavokine, N. Electron cooling in graphene enhanced by plasmon–hydron resonance. *Nat. Nanotechnology* **2023**, *18*, 898–904.

(18) Nalige, S. S.; Galonska, P.; Kelich, P.; Sistemich, L.; Herrmann, C.; Vukovic, L.; Kruss, S.; Havenith, M. Fluorescence changes in carbon nanotube sensors correlate with THz absorption of hydration. *Nat. Commun* **2024**, *15*, 6770.

(19) Siro Brigiano, F.; Gierada, M.; Tielens, F.; Pietrucci, F. Mechanism and Free-Energy Landscape of Peptide Bond Formation at the Silica–Water Interface. *ACS Catal.* **2022**, *12*, 2821–2830.

(20) Dubouis, N.; Serva, A.; Berthin, R.; Jeanmairet, G.; Porcheron, B.; Salager, E.;

Salanne, M.; Grimaud, A. Tuning water reduction through controlled nanoconfinement within an organic liquid matrix. *Nat. Catal.* **2020**, *3*, 656–663.

(21) Rego, N. B.; Patel, A. J. Understanding hydrophobic effects: Insights from water density fluctuations. *Annual Review of Condensed Matter Physics* **2022**, *13*, 303–324.

(22) Xi, E.; Venkateshwaran, V.; Li, L.; Rego, N.; Patel, A. J.; Garde, S. Hydrophobicity of proteins and nanostructured solutes is governed by topographical and chemical context. *Proc. Natl. Acad. Sci.* **2017**, *114*, 13345–13350.

(23) Mamatkulov, S. I.; Khabibullaev, P. K.; Netz, R. R. Water at hydrophobic substrates: curvature, pressure, and temperature effects. *Langmuir* **2004**, *20*, 4756–4763.

(24) Jiao, S.; Shell, M. S. Inverse design of pore wall chemistry and topology through active learning of surface group interactions. *J. Chem. Phys.* **2024**, *160*, 124705.

(25) Rego, N. B.; Ferguson, A. L.; Patel, A. J. Learning the relationship between nanoscale chemical patterning and hydrophobicity. *Proc. Natl. Acad. Sci.* **2022**, *119*, e2200018119.

(26) Giovambattista, N.; Lopez, C. F.; Rossky, P. J.; Debenedetti, P. G. Hydrophobicity of protein surfaces: Separating geometry from chemistry. *Proc. Natl. Acad. Sci.* **2008**, *105*, 2274–2279.

(27) Monroe, J.; Barry, M.; DeStefano, A.; Gokturk, P. A.; Jiao, S.; Robinson-Brown, D.; Webber, T.; Crumlin, E. J.; Han, S.; Shell, M. S. Water Structure and Properties at Hydrophilic and Hydrophobic Surfaces. *Ann. Rev. Chem. Biomolec. Eng:* **2020**, *11*, null.

(28) Cyran, J. D.; Donovan, M. A.; Vollmer, D.; Brigiano, F. S.; Pezzotti, S.; Galimberti, D. R.; Gaigeot, M.-P.; Bonn, M.; Backus, E. H. G. Molecular hydrophobicity at a macroscopically hydrophilic surface. *Proc. Natl. Acad. Sci. U.S.A.* **2019**, *116*, 1520–1525.

(29) Chen, W.; Kroutil, O.; Předota, M.; Pezzotti, S.; Gaigeot, M.-P. Wetting of a Dynamically Patterned Surface Is a Time-Dependent Matter. *J. Phys. Chem. B.* **2024**, *128*, 11914–11923.

(30) Du, Q.; Freysz, E.; Shen, Y. R. Surface vibrational spectroscopic studies of hydrogen bonding and hydrophobicity. *Science* **1994**, *264*, 826–828.

(31) Chen, W.; Sanders, S. E.; Ozdamar, B.; Louaas, D.; Brigiano, F. S.; Pezzotti, S.; Petersen, P. B.; Gaigeot, M.-P. On the trail of molecular hydrophilicity and hydrophobicity at aqueous interfaces. *J. Phys. Chem. Lett.* **2023**, *14*, 1301–1309.

(32) Murke, S.; Chen, W.; Pezzotti, S.; Havenith, M. Tuning Acid–Base Chemistry at an Electrified Gold/Water Interface. *J. Am. Chem. Soc.* **2024**, *146*, 12423–12430.

(33) Liang, H.-Q.; Zhao, S.; Hu, X.-M.; Ceccato, M.; Skrydstrup, T.; Daasbjerg, K. Hydrophobic copper interfaces boost electroreduction of carbon dioxide to ethylene in water. *ACS Catal.* **2021**, *11*, 958–966.

(34) Rotenberg, B.; Patel, A. J.; Chandler, D. Molecular explanation for why talc surfaces can be both hydrophilic and hydrophobic. *J. Am. Chem. Soc.* **2011**, *133*, 20521–20527.

(35) Qu, M.; Huang, G.; Liu, X.; Nie, X.; Qi, C.; Wang, H.; Hu, J.; Fang, H.; Gao, Y.; Liu, W.-T.; others Room temperature bilayer water structures on a rutile TiO 2 (110) surface: hydrophobic or hydrophilic? *Chem. Sci.* **2022**, *13*, 10546–10554.

(36) Chen, Y.-W.; Chu, I.-H.; Wang, Y.; Cheng, H.-P. Water thin film-silica interaction on α-quartz (0001) surfaces. *Phys. Rev. B* **2011**, *84*, 155444.

(37) Willard, A. P.; Reed, S. K.; Madden, P. A.; Chandler, D. Water at an electrochemical interface—a simulation study. *Faraday discussions* **2009**, *141*, 423–441.

(38) Eggert, T.; Hörmann, N. G.; Reuter, K. Cavity formation at metal–water interfaces. *J. Chem. Phys.* **2023**, *159*.

(39) Bin Jassar, M.; Yao, Q.; Siro Brigiano, F.; Chen, W.; Pezzotti, S. Chemistry at Oxide/Water Interfaces: The Role of Interfacial Water. *J. Phys. Chem. Lett.* **2024**, *15*, 11961–11968.

(40) Serva, A.; Havenith, M.; Pezzotti, S. The role of hydrophobic hydration in the free energy of chemical reactions at the gold/water interface: Size and position effects. *J. Chem. Phys.* **2021**, *155*, 204706.

(41) Li, P.; Jiang, Y.; Hu, Y.; Men, Y.; Liu, Y.; Cai, W.; Chen, S. Hydrogen bond network connectivity in the electric double layer dominates the kinetic pH effect in hydrogen electrocatalysis on Pt. *Nat. Catal.* **2022**, *5*, 900–911.

(42) Serva, A.; Pezzotti, S. S.O.S: Shape, orientation, and size tune solvation in electrocatalysis. *J. Chem. Phys.* **2024**, *160*, 094707.

(43) Yoo, J. M.; Ingenmey, J.; Salanne, M.; Lukatskaya, M. R. Anion effect in electrochemical CO2 reduction: from spectators to orchestrators. *J. Am. Chem. Soc.* **2024**,

(44) Azimzadeh Sani, M.; Pavlopoulos, N. G.; Pezzotti, S.; Serva, A.; Cignoni, P.; Linnemann, J.; Salanne, M.; Gaigeot, M.-P.; Tschulik, K. Unexpectedly high capacitance of the metal nanoparticle/water interface: molecular-level insights into the electrical double layer. *Angew. Chem.* **2022**, *134*, e202112679.

(45) Zhang, X.-L.; Yu, P.-C.; Sun, S.-P.; Shi, L.; Yang, P.-P.; Wu, Z.-Z.; Chi, L.-P.; Zheng, Y.-R.; Gao, M.-R. In situ ammonium formation mediates efficient hydrogen production from natural seawater splitting. *Nat. Commun* **2024**, *15*, 9462.

(46) Marin-Laflèche, A.; Haefele, M.; Scalfi, L.; Coretti, A.; Dufils, T.; Jeanmairet, G.; Reed, S. K.; Alessandra, S.; Berthin, R.; Bacon, C.; others MetalWalls: A classical molecular dynamics software dedicated to the simulation of electrochemical systems. *J. Open Source Softw.* **2020**, *5*, 2373.

(47) Serva, A.; Scalfi, L.; Rotenberg, B.; Salanne, M. Effect of the metallicity on the capacitance of gold–aqueous sodium chloride interfaces. *J. Chem. Phys.* **2021**, *155*.

(48) Patel, A. J.; Varilly, P.; Chandler, D. Fluctuations of Water near Extended Hydrophobic and Hydrophilic Surfaces. *J. Phys. Chem. B* **2010**, *114*, 1632–1637.

(49) Dazas, B.; Jiménez-Ruiz, M.; Grégoire, B.; Hubert, F.; Lanson, B.; Tertre, E.; Michot, L.; Ferrage, E. Molecular Hydrophobicity Signature in Charged Bidimensional Clay Materials. *J. Phys. Chem. A* **2024**,

(50) Scalfi, L.; Dufils, T.; Reeves, K. G.; Rotenberg, B.; Salanne, M. A semiclassical Thomas–Fermi model to tune the metallicity of electrodes in molecular simulations. *J. Chem. Phys.* **2020**, *153*.

(51) Michaelides, A.; Ranea, V. A.; de Andres, P. L.; King, D. A. General Model for Water Monomer Adsorption on Close-Packed Transition and Noble Metal Surfaces. *Phys. Rev. Lett.* **2003**, *90*, 216102.

(52) Heinz, H.; Vaia, R.; Farmer, B.; Naik, R. Accurate simulation of surfaces and interfaces of face-centered cubic metals using 12- 6 and 9- 6 Lennard-Jones potentials. *J. Phys. Chem. C* **2008**, *112*, 17281–17290.

(53) Bañuelos, J. L.; Borguet, E.; Brown Jr, G. E.; Cygan, R. T.; DeYoreo, J. J.; Dove, P. M.; Gaigeot, M.-P.; Geiger, F. M.; Gibbs, J. M.; Grassian, V. H.; others Oxide–and silicate–water interfaces and their roles in technology and the environment. *Chem. Rev.* **2023**, *123*, 6413–6544.

(54) Wang, R.; Zou, Y.; Remsing, R. C.; Ross, N. O.; Klein, M. L.; Carnevale, V.; Borguet, E. Superhydrophilicity of α-alumina surfaces results from tight binding of interfacial waters to specific aluminols. *J. Colloid Interface Sci.* **2022**, *628*, 943–954.

(55) Pezzotti, S.; Serva, A.; Sebastiani, F.; Brigiano, F. S.; Galimberti, D. R.; Potier, L.; Alfarano, S.; Schwaab, G.; Havenith, M.; Gaigeot, M.-P. Molecular fingerprints of hydrophobicity at aqueous interfaces from theory and vibrational spectroscopies. *J. Phys. Chem. Lett.* **2021**, *12*, 3827–3836.

(56) Remsing, R. C.; Weeks, J. D. Hydrophobicity scaling of aqueous interfaces by an electrostatic mapping. *J. Phys. Chem. B* **2015**, *119*, 9268–9277.

(57) Shin, S.; Willard, A. P. Quantifying the molecular polarization response of liquid water interfaces at heterogeneously charged surfaces. *J. Chem. Theory Comput.* **2023**, *19*, 1843–1852.

(58) Shin, S.; Willard, A. P. Water's interfacial hydrogen bonding structure reveals the effective strength of surface–water interactions. *J. Phys. Chem. B* **2018**, *122*, 6781–6789.

(59) Patel, A. J.; Varilly, P.; Chandler, D. Fluctuations of water near extended hydrophobic and hydrophilic surfaces. *J. Phys. Chem. B* **2010**, *114*, 1632–1637.

(60) Berendsen, H. J. C.; Grigera, J. R.; Straatsma, T. P. The Missing Term in Effective Pair Potentials. *J. Phys. Chem.* **1987**, *91*, 6269–6271.

(61) Luzar, A.; Chandler, D. Structure and hydrogen bond dynamics of water–dimethyl sulfoxide mixtures by computer simulations. *J. Chem. Phys.* **1993**, *98*, 8160–8173.